https://doi.org/10.3311/PPtr.40046
Creative Commons Attribution

Periodica Polytechnica Transportation Engineering

Process-property Relationships in Fused Filament Fabrication of 17-4PH Stainless Steel: Effects of Printing Parameters on Tensile Strength, Shrinkage, and Defect-sensitive Behavior

György Ledniczky[1], Adrián Bognár[1], Krisztián Kun[1*]

[1] Department of Innovative Vehicles and Materials, GAMF Faculty Engineering and Computer Science, John von Neumann University, H-6000 Kecskemét, Izsáki st. 10., Hungary
[*] Corresponding author, e-mail: kun.krisztian@nje.hu

Received: 31 January 2025, Accepted: 21 April 2026, Published online: 16 November 2026

Abstract

This study investigates the effect of selected Fused Filament Fabrication parameters on the tensile behavior and dimensional change of 17-4PH stainless steel specimens produced from BASF Ultrafuse filament. Layer height, printing speed, and infill angle were evaluated using a Taguchi-based experimental design, while the printed parts were subsequently subjected to catalytic debinding and sintering. Tensile testing of the as-sintered specimens showed that the best-performing parameter combination reached 802 MPa, corresponding to approximately 80% of the tensile strength reported by the material supplier. The statistical analysis identified layer height as the most influential factor, followed by infill angle, whereas printing speed had a smaller effect within the investigated range. In addition to the primary tensile and shrinkage evaluation, supplementary dimensional, density-related, and fracture-surface observations were used to support the interpretation of the results. These findings indicate that the final mechanical response cannot be explained solely by nominal printing settings, but must be understood through their effect on green-part integrity, densification, shrinkage, and internal defect formation during post-processing. Overall, the results show that the performance of extrusion-based 17-4PH stainless steel parts is governed by the combined effect of deposition strategy and thermal treatment, and that reliable parameter selection can significantly improve the mechanical quality of sintered components.

Keywords

Fused Filament Fabrication, metal FFF, 17-4PH stainless steel, shrinkage, process parameters

1 Introduction

Additive manufacturing has attracted increasing attention in engineering because it enables the production of geometries that are difficult, costly, or even impossible to obtain by conventional subtractive or mold-based methods [Alami et al., 2023; Wohlers Associates, 2017]. Within metal additive manufacturing, powder-bed and related high-energy processes still dominate both industrial adoption and the scientific literature, while extrusion-based routes have emerged as more accessible alternatives for the fabrication of metal components [Nurhudan et al., 2021; Suwanpreecha and Manonukul, 2022]. The conceptual roots of extrusion-based shaping of particle-filled feedstocks can be traced back to earlier work on ceramics and metal-containing materials, which established the feasibility of layerwise deposition followed by thermal consolidation [Allahverdi et al., 2001; Wu et al., 2002]. Compared with powder-based methods, material extrusion of metal-filled filaments offers a lower entry barrier in terms of machine cost, handling requirements, and operational safety [Galantucci et al., 2022; Suwanpreecha and Manonukul, 2022]. However, this advantage is accompanied by a more complex manufacturing route, because the printed component is only an intermediate green part containing a substantial amount of binder. In order to obtain the final metallic part, the specimen must undergo debinding and sintering, similarly to the workflow of metal injection molding [German, 2019; Singh et al., 2021; Galantucci et al., 2022]. As a result, the final behavior of the part is governed not only by the deposition strategy, but also by binder removal, densification, shrinkage, and the formation or retention of internal defects during post-processing [Thompson et al., 2019; Liu et al., 2020; Zhang and Roch, 2022]. This makes metal FFF a process chain problem rather than a purely printing-related one. Among the stainless steels applicable to

Cite this article as: Ledniczky Gy., Bognár, A., Kun, K. (2026) "Process-property Relationships in Fused Filament Fabrication of 17-4PH Stainless Steel: Effects of Printing Parameters on Tensile Strength, Shrinkage, and Defect-sensitive Behavior", Periodica Polytechnica Transportation Engineering, https://doi.org/10.3311/PPtr.40046

this route, 17-4PH is particularly important because of its favorable combination of strength, hardness, and corrosion resistance, as well as its broad engineering relevance [Cho et al., 2023; Kedziora et al., 2022]. Recent studies have shown that extrusion-based additive manufacturing can produce 17-4PH components with promising mechanical properties, especially when printing, sintering, and subsequent heat treatment are properly controlled [Henry et al., 2021; Pellegrini et al., 2023]. At the same time, the literature consistently indicates that the attainable strength remains strongly dependent on porosity, incomplete densification, and the integrity of the deposited filament structure [Galantucci et al., 2022; Singh et al., 2021; Zhang and Roch, 2022]. This is particularly relevant in filament-based processing, where the orientation of deposited roads, the degree of inter-road contact, and the green-part homogeneity may later influence shrinkage uniformity and defect sensitivity during thermal treatment [Thompson et al., 2019; Godec et al., 2020; Cho et al., 2023].

Several previous studies provide an important basis for the present work. Godec et al. (2020) investigated the effect of printing parameters on the tensile properties of FFF-manufactured 17-4PH stainless steel and demonstrated that parameter selection plays a measurable role in the mechanical response of the final parts. Singh et al. (2021) analyzed the printing, debinding, and sintering stages of 17-4PH feedstock and highlighted the importance of proper filling and densification behavior. Zhang and Roch (2022) reported that sintered 17-4PH parts produced by fused filament fabrication can approach high strength levels, but they also underlined the process sensitivity associated with shrinkage and final part quality. More broadly, review studies have emphasized that porosity and defect formation remain among the principal limiting factors in extrusion-based metal additive manufacturing [Galantucci et al., 2022; Nurhudan et al., 2021].

Accordingly, the aim of the present study is to investigate the influence of selected Fused Filament Fabrication parameters on the tensile behavior and dimensional change of 17-4PH stainless steel specimens produced from bound-metal filament. Particular emphasis is placed on layer height, printing speed, and infill angle, because these parameters directly affect deposition quality, local bonding conditions, and the internal architecture of the green part prior to debinding and sintering [Godec et al., 2020; Singh et al., 2021; Zhang and Roch, 2022].

By combining a Taguchi-based experimental design with tensile testing and shrinkage analysis, the study aims not only to identify favorable parameter sets, but also to provide a more physically grounded interpretation of the resulting process–property relationships in defect-sensitive metal FFF.

2 Materials and methods

The experimental work was carried out using BASF Ultrafuse 17-4PH filament as the bound-metal feedstock. This material consists of 17-4PH stainless steel powder embedded in a polymer-based binder system and is intended for a shaping–debinding–sintering process route (Figs. 1 and 2) that is closely related to metal injection molding [German, 2019; Galantucci et al., 2022; Singh et al., 2021]. The metallic phase is a precipitation-hardening martensitic stainless steel widely used in engineering applications requiring a favorable combination of strength, hardness, and corrosion resistance [Cho et al., 2023; Kedziora et al., 2022].

2.1 Feedstock, printing system, and specimen concept

Printing was performed on a CraftBot IDEX XL system using CraftWare slicing software. The specimen geometry was selected to represent a tensile-test-compatible form

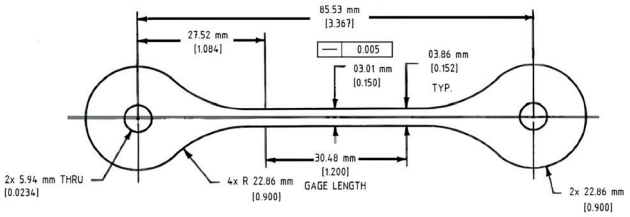


Fig. 1 Geometry of the tensile specimen and reference dimensions used for shrinkage evaluation

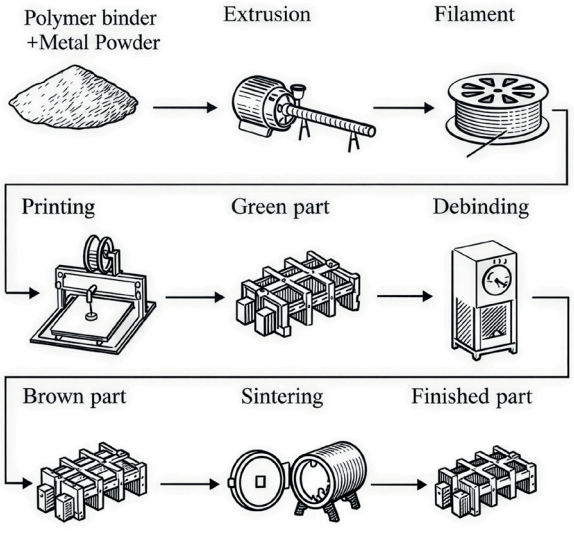


Fig. 2 Process route of filament-based metal additive manufacturing applied in the present study

while also enabling dimensional evaluation before and after post-processing. For this reason, the printed parts included reference holes whose center-to-center distance could be measured in both the green and sintered states. In addition to dimensional measurements, the mass of each green specimen was recorded prior to debinding and sintering. This approach made it possible to evaluate not only tensile behavior, but also the dimensional and mass changes associated with the post-processing route.

2.2 Printing strategy and design of experiments

The study was designed to examine the influence of three deposition-related process parameters on the final performance of the sintered parts: layer height, printing speed, and infill angle. These parameters were selected because they directly affect filament placement, inter-road contact, build time, and the internal architecture of the green part, and therefore may also influence densification and defect formation during subsequent thermal treatment [Godec et al., 2020; Singh et al., 2021; Zhang and Roch, 2022]. Preliminary results of this study were presented at the 39th Colloquium on Advanced Manufacturing and Repair Technologies in Vehicle Industry [Ledniczky et al., 2024].

A Taguchi L9 orthogonal array was used in order to evaluate the main effects of the selected factors with a limited number of experimental runs. The investigated parameter levels were as follows: layer height 0.2, 0.3, and 0.4 mm; printing speed 15, 25, and 35 mm/s; and infill angle 0°, 45°, and 90°. In all cases, the specimens were produced with 100% infill, and the internal pattern consisted of parallel raster lines, while the raster orientation varied according to the selected infill angle. Prior to the final experimental campaign, preliminary trial prints were carried out to define a stable printing window and to avoid unacceptable printing defects such as poor first-layer adhesion or nozzle jamming. After fabrication, the green parts were visually inspected, weighed individually, and measured at the reference holes before being sent for post-processing.

2.3 Catalytic debinding

Since the selected feedstock requires industrial debinding and sintering conditions, the printed green parts were post-processed by an external service provider using a BASF-compatible catalytic debinding route for Catamold-type binder systems. In this stage, the furnace chamber was heated to 120 °C and held for 45 min. After this preheating step, acid exposure was applied for approximately 1 h per 1 mm wall thickness at a flow rate of 3.4 ml/min. This was followed by an additional 90 min hold at 120 °C in order to complete the primary binder-removal stage and prepare the furnace for unloading.

The purpose of catalytic debinding was to remove the primary binder component while maintaining sufficient structural integrity for the subsequent thermal treatment. After this step, the specimens were converted from green parts to brown parts.

At this stage, the components had already undergone a partial mass reduction and became more fragile, but retained enough cohesion to be transferred to the sintering stage (Fig. 3). Because binder removal can strongly influence internal pore evolution and shape stability, catalytic debinding was treated as a critical part of the overall process chain rather than as a separate auxiliary step [Thompson et al., 2019; Galantucci et al., 2022].

2.4 Thermal binder removal and sintering

Following catalytic debinding, the brown parts were subjected to a combined thermal debinding and sintering cycle. First, the temperature was raised to 450 °C at a heating rate of 5 °C/min and held for 150 min. The furnace was then heated to 600 °C at 3 °C/min and held for 60 min. Finally, the sintering stage was carried out at 1,380 °C, reached at a heating rate of 5 °C/min and maintained for 180 min, after which the parts were allowed to cool to room temperature.

This multi-stage thermal route was used to remove the remaining binder constituents and to consolidate the powder skeleton into the final metallic structure (Fig. 4). During this stage, the most significant dimensional contraction

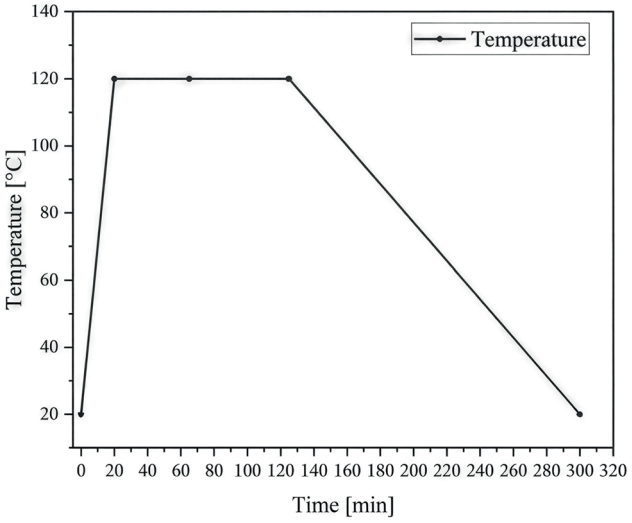


Fig. 3 Catalytic debinding cycle used for the primary binder-removal step

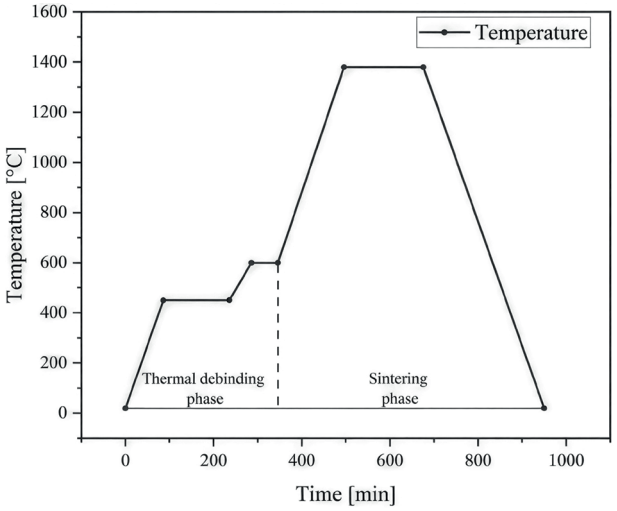


Fig. 4 Thermal debinding and sintering cycle applied after catalytic debinding

occurred, and the final mechanical behavior of the parts was established through densification, shrinkage, and the possible retention or development of internal defects. For this reason, the thermal cycle was regarded as an integral contributor to the final process–property relationship, rather than merely a finishing operation [Singh et al., 2021; Zhang and Roch, 2022].

2.5 Mechanical testing and dimensional measurements

After post-processing, the specimens were evaluated in the as-sintered condition, without machining or surface finishing. Tensile tests were carried out on an Instron 5900R 4482 universal testing machine equipped with a 100 kN load cell. The maximum tensile stress obtained from these tests was used as the primary response variable in the Taguchi-based statistical evaluation.

In parallel with mechanical testing, the linear shrinkage of the parts was determined from the change in the measured hole-to-hole distance between the green and sintered states. Mass change during post-processing was also assessed by comparing the weight of the specimens before and after the debinding–sintering route. In this way, the experimental methodology linked the tensile response of the final parts (Fig. 5) to the process chain through both mechanical and dimensional indicators.

2.6 Complementary characterization methods

To support the interpretation of the primary BASF Ultrafuse 17-4PH parameter study, additional results from a complementary 17-4PH material-extrusion dataset were incorporated into the present work. These supplementary results included GOM-based dimensional evaluation,

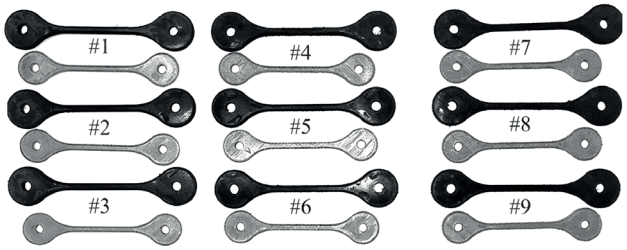


Fig. 5 Representative green and sintered specimens after post-processing

density and fill-ratio estimation based on pycnometric measurements, and optical examination of representative fracture surfaces after tensile testing. Since these data were obtained from a different but technologically comparable 17-4PH feedstock system, they were not included in the Taguchi optimization itself and were not used for direct statistical merging with the BASF-based experiments. Instead, they were used as complementary evidence to support the interpretation of shrinkage behavior, densification trends, internal heterogeneity, and defect formation in extrusion-based metal additive manufacturing.

The additional dimensional analysis was used to refine the interpretation of sintering-induced shrinkage and scaling behavior, while the density-related results were considered to evaluate the extent of consolidation achieved during post-processing. Fracture-surface observations were included in order to provide direct visual information on pore distribution, incomplete bonding, and local structural discontinuities. Together, these supplementary characterizations were used to extend the process–property interpretation beyond the nominal printing parameters and to provide a more physically grounded explanation of the measured tensile behavior.

3 Experimental design

To analyze the combined effect of the selected Fused Filament Fabrication parameters without performing a full-factorial campaign, a Taguchi-based design of experiments was adopted. This approach was chosen because it allows a structured evaluation of the main process factors with a limited number of experimental runs, which is particularly advantageous in metal filament printing, where both the feedstock and the post-processing route are costly and time-consuming [Singh et al., 2021]. In the revised concept of the present study, the experimental design was not treated as a simple parameter-screening exercise, but as a framework for linking green-part quality to the final tensile response and dimensional change of the sintered specimens.

Based on preliminary printing trials and literature findings, three controllable factors were selected: layer height, printing speed, and infill angle. These parameters were chosen because they directly influence filament deposition quality, local inter-road bonding, printing stability, and the internal architecture of the green part, which may later affect shrinkage behavior and defect sensitivity during debinding and sintering [Godec et al., 2020; Singh et al., 2021; Zhang and Roch, 2022]. Preliminary trials were used to define a stable processing window. Outside this window, insufficient first-layer adhesion and occasional filament jamming were observed, therefore the final experimental levels were selected from the reliably printable range established before the main test series, as seen in Table 1 [BASF ForwardAM].

An L9 orthogonal array was applied, in which each factor was investigated at three levels. The selected levels were 0.2, 0.3, and 0.4 mm for layer height; 15, 25, and 35 mm/s for printing speed; and 0°, 45°, and 90° for infill angle. All specimens were printed with 100% infill, while the raster pattern consisted of parallel lines whose orientation was varied according to the assigned infill angle. The resulting nine parameter combinations are summarized in Table 1. This arrangement provided a balanced and efficient basis for evaluating the relative importance of the selected factors while keeping the number of experiments at a manageable level.

The purpose of the design was to identify parameter combinations that improve the tensile performance of the sintered parts while also accounting for dimensional stability. Accordingly, the experimental outputs considered in the subsequent evaluation were maximum tensile stress and linear shrinkage. Tensile strength was treated as a "larger is better" response in the Taguchi analysis, whereas shrinkage was interpreted as a complementary indicator of post-processing behavior rather than as a standalone optimization target. In this way, the experimental design supported the new process–property focus of the study by relating deposition settings to the final mechanical response through the intermediate effects of green-part integrity, post-processing sensitivity, and dimensional change.

Table 1 Printing parameter combinations used in the L9 orthogonal array

Experiment	Layer height [mm]	Printing speed [mm/s]	Infill angle [°]
1.	0.2	15	0
2.	0.2	25	45
3.	0.2	35	90
4.	0.3	15	45
5.	0.3	25	90
6.	0.3	35	0
7.	0.4	15	90
8.	0.4	25	0
9.	0.4	35	45

In addition to the primary Taguchi-based parameter study, supplementary characterization methods were applied to support the interpretation of shrinkage, densification, and defect-sensitive mechanical behavior.

4 Results

After catalytic debinding and sintering, the specimens were tested in the as-sintered condition, without machining or surface finishing.

4.1 Thermal binder removal and sintering

Linear shrinkage was evaluated from the change in the measured hole-to-hole distance between the green and sintered states, while tensile testing was performed on an Instron 5900R 4482 universal testing machine equipped with a 100 kN load cell. For comparison of the mechanical response, the best-performing specimen from each investigated layer-height group was selected, and the corresponding load-extension curves are shown in Fig. 6. Among the investigated parameter combinations, Experiment 2 exhibited the highest tensile stress, reaching 802 MPa. This value corresponds to approximately 80% of the tensile strength reported in the BASF datasheet for the material, despite the fact that the specimens were tested in the as-sintered condition and not in a machined state [BASF ForwardAM]. As seen in Fig. 6, Experiment 2 also showed the most favorable overall tensile response among the highlighted conditions,

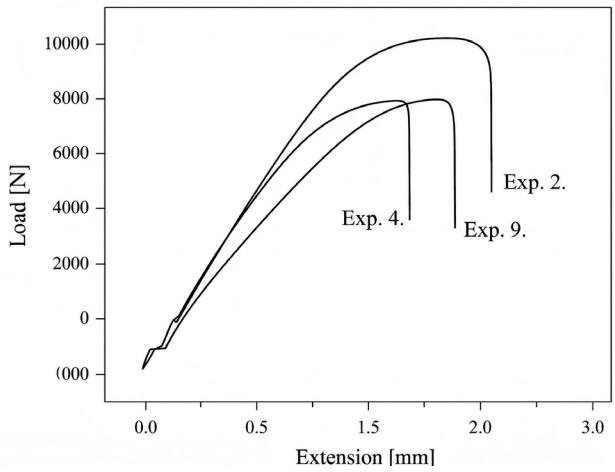


Fig. 6 Representative load-extension curves of the best-performing specimens selected from the investigated layer-height groups (Experiments 2, 4, and 9)

whereas Experiments 4 and 9 reached lower maximum load levels and failed at smaller extensions. The shape of the curves suggests that the difference between the tested conditions cannot be interpreted only as a change in nominal strength level, but also as a difference in structural continuity and defect sensitivity during loading.

4.2 Taguchi-based evaluation of the main process parameters

The tensile results were further analyzed using the Taguchi method with the "larger is better" criterion in order to identify the relative significance of the selected process parameters. The corresponding mean performance values are summarized in Table 2. According to the response table, layer height had the strongest effect on tensile strength, with a delta value of 163.6, followed by infill angle with 85.6, whereas printing speed had the smallest influence within the investigated parameter window, with a delta value of 60.9. Based on the factor-level averages, the most favorable levels were 0.2 mm for layer height, 15 mm/s for printing speed, and 45° for infill angle.

The calculation can be described by the following Eq. (1):

$$MSD_i = \frac{\sum_{j=1}^{n} \frac{1^n}{y_{ij}^2}}{n} \tag{1}$$

MSD_i - the mean squared deviation,
i - the number of the experiment,
y_{ij} - the j-th value measured for setting type i,
n - the number of replicates.

Based on Eq. (1), the noise in the experiment was filtered so that, as expected, the higher values are the better (higher tensile stress). The results obtained are given in Table 2.

The main-effects plot derived from the Taguchi evaluation is shown in Fig. 7. A pronounced reduction in average tensile strength was observed when the layer height increased from 0.2 to 0.3 mm, followed by a partial recovery at 0.4 mm. In contrast, the influence of printing speed was more moderate and showed an overall decreasing tendency with increasing speed. The infill-angle response exhibited a clear maximum at 45°, while both 0° and 90° resulted in lower average tensile strength. As seen in Fig. 7, the tensile response was therefore more sensitive to geometric deposition conditions than to deposition rate itself.

Table 2 Taguchi response table based on average tensile strength values

Level	Layer height [mm]	Printing speed [mm/s]	Infill angle [°]
1	744.4	674.8	619.1
2	580.9	657.8	704.7
3	621.1	613.9	622.7
Delta	163.6	60.9	85.6
Rank	1	3	2

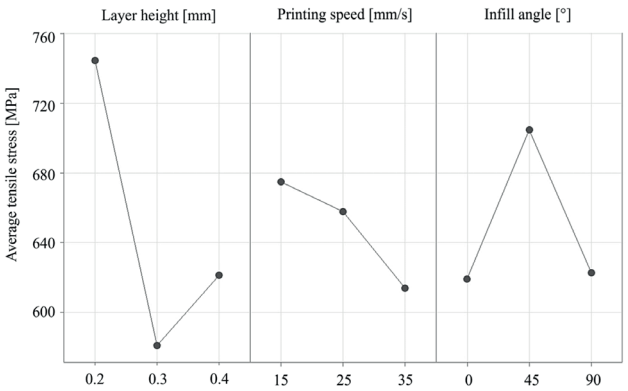


Fig. 7 Main-effects plot for average tensile strength as a function of layer height, printing speed, and infill angle

To further examine the interaction between the two most influential factors, a second-order response-surface model was generated after coding the variables into the range from −1 to +1 in Minitab. The general form of the regression model is given in Eq. (2), and the resulting contour plot is presented in Fig. 8. The response surface confirms that the most favorable tensile-strength region is associated with lower layer heights and intermediate infill angles. As seen in Fig. 8, the highest response is located approximately in the range of 0.20–0.25 mm layer height and around 45–55° infill angle, whereas larger layer heights combined with low infill angles are associated with reduced tensile strength.

This result is consistent with both the response table and the main-effects diagram.

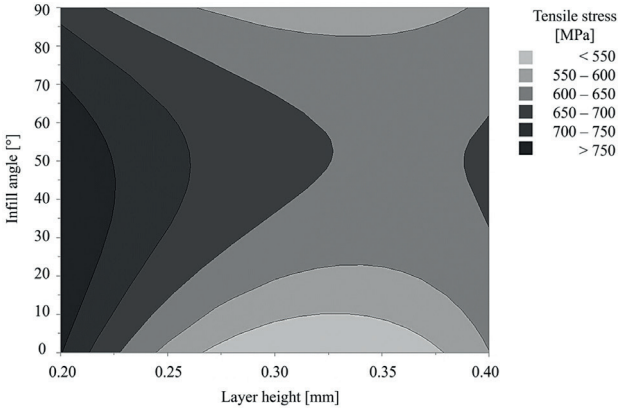


Fig. 8 Response-surface contour plot showing the combined effect of layer height and infill angle on tensile strength

The second-order regression Eq. (2) is as follows:

$$Y = \beta_0 + \sum_{i=1}^{k} \beta_i x_i + \sum_{i=1}^{k} \beta_{ii} x_i^2 + \sum_{i=1}^{k-1} \sum_{j=i+1}^{k} \beta_{ij} x_i x_j + \varepsilon \quad (2)$$

Y - the response variable,
β_0 - the constant and β_1, β_2, ..., β_k are the coefficients,
x_1, x_2, ..., x_k - the values of the terms,
ε - the error term.

Overall, the statistical evaluation indicates that the best mechanical performance within the tested design space was achieved not simply by maximizing deposition efficiency, but by selecting a parameter set that promotes a more favorable green-part architecture prior to debinding and sintering. In this respect, layer height was identified as the dominant control factor, infill angle as the second most important parameter, and printing speed as the least influential factor within the examined range.

4.3 Dimensional change and shrinkage behavior

To support the interpretation of the hole-distance measurements obtained on the BASF-based specimens, complementary dimensional observations were considered from an additional 17-4PH material-extrusion series evaluated by GOM-based measurement (Zeiss GOM ScanCobot). The results (Fig. 9) confirmed that the dimensional change after sintering is substantial and process-dependent. In the preliminary series, the measured shrinkage of the sintered parts was 14.951%, 15.380%, and 14.902% for the investigated conditions, with an average value of 15.078%. Based on these data, scaling factors of Z_{x-y}= 1.1775 and Z_Z = 1.1249 were calculated for geometry compensation.

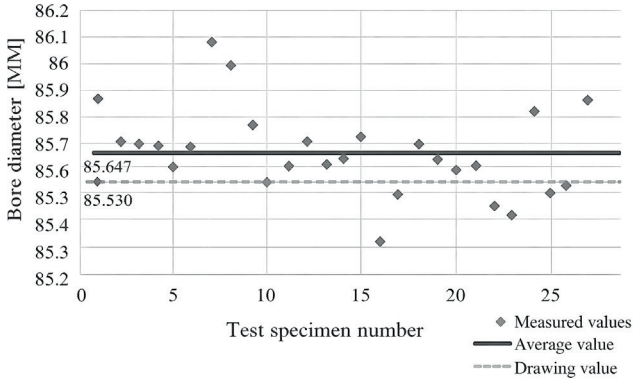


Fig. 9 Dimensional evaluation of sintered specimens and measured shrinkage values determined from hole-distance measurements

These results indicate that shrinkage should not be treated as a fixed nominal material property, but rather as a process-dependent outcome influenced by the integrity and homogeneity of the green structure. The observed magnitude of dimensional contraction is consistent with the general behavior reported for extrusion-based metal additive manufacturing [Thompson et al., 2019; Singh et al., 2021; Zhang and Roch, 2022]. In the context of the present study, this means that the tensile results must be interpreted together with the dimensional response, since the same deposition-related conditions that influence mechanical performance also affect the way the structure contracts during sintering.

4.4 Density development and fill ratio after sintering

A complementary view of specimen consolidation was obtained from gas pycnometry. The density measurements were performed using an AccuPyc II 1340 instrument, yielding a filament density of $\rho_{filament}$ = 5.2898 g/cm^3, while the reference density used for the sintered 17-4PH material was ρ_{7-4PH} = 7.750 g/cm^3. On this basis, the fill ratio of the parts could be estimated before and after post-processing. The calculated results (Fig. 10) showed that sintering increased the average fill ratio by 3.24%, with the smallest increase being 2.21% and the largest 3.75% across the investigated series.

As seen in Fig. 10, the densification trend after sintering was favorable, but the magnitude of improvement remained limited. This suggests that the final state of the specimens was still strongly dependent on the packing quality and continuity already established in the green condition. In other words, post-processing improved consolidation, but it did not fully eliminate the structural consequences of insufficient local filling or discontinuous filament arrangement. This interpretation is in agreement

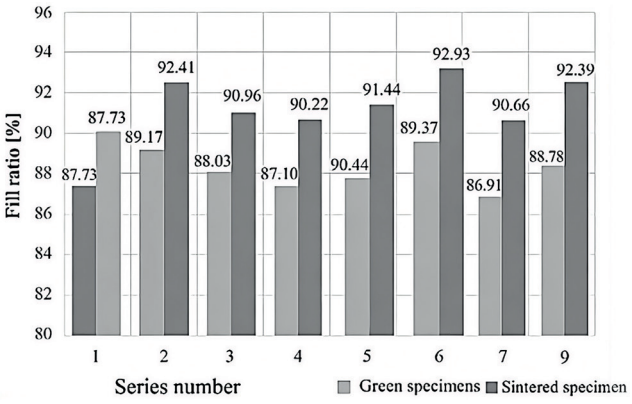


Fig. 10 Calculated density and fill-ratio development of 17-4PH specimens before and after sintering

with the tensile results of the present BASF-based study, where the most favorable mechanical response was associated with the parameter combination most likely to support a denser and more coherent green-part structure.

4.5 Mechanical scatter and fracture-surface observations

Additional insight into the tensile behavior was provided by comparative tensile diagrams (Fig. 11) and fracture-surface microscopy from a complementary 17-4PH material-extrusion series. The lower-performing specimens exhibited markedly smaller elongation before failure, which is consistent with the presence of internal heterogeneity, larger pores, or local discontinuities acting as stress concentrators. In one case, a partial fracture was already visible after the plastic-deformation stage, indicating that a local structural defect had reduced the effective load-bearing cross-section. By contrast, such irregular behavior was not apparent in the highest-performing specimens.

Fracture-surface microscopy further clarified the defect-sensitive nature of the mechanical response. Representative optical micrographs revealed regions with relatively continuous sintered structure interrupted by visible pores, as well as areas where the connection between neighboring regions was incomplete or entirely absent. In several cases, the outer shell did not form a fully coherent bond after sintering, and local separation of the upper layers could also be observed, as seen in Fig. 12. Material-deficient regions were visible in the central part of the cross-section, indicating that the final structural continuity of the specimens was locally compromised.

The fracture-surface observations also suggest that at least a part of the final defect population originated before thermal treatment. Signs of local discontinuity were already detectable at the slicing stage, where small gaps could be identified between adjacent deposited roads. Although these gaps appeared limited in the digital model, their structural significance increased during debinding and sintering, and they evolved into larger connected voids in the final specimen. This indicates that the measured mechanical behavior was governed by the coupled effect of deposition quality and post-processing, rather than by either stage alone.

4.6 Integrated interpretation of the process-property relationship

Taken together, the tensile, statistical, dimensional, density-related, and fracture-surface results indicate that the final performance of extrusion-based 17-4PH parts is controlled by the full process chain. The Taguchi analysis identified the most influential nominal parameters, but the complementary observations show why these factors matter physically: they influence green-part integrity, local packing quality, and the tendency for internal discontinuities to persist or amplify during debinding and sintering. Thus, the measured parameter effects should not be interpreted as isolated print-stage effects only, but as indirect manifestations of how the chosen deposition strategy governs densification, shrinkage behavior, and defect evolution in the final metallic component

5 Discussion

The results show that the tensile performance of Fused Filament Fabricated 17-4PH stainless steel is controlled by the combined effect of printing conditions and subsequent thermal post-processing. Although the Taguchi analysis identified layer height as the most influential factor, followed by infill angle and then printing speed, these parameters should not be interpreted only as nominal settings. Their importance lies in how they affect the architecture and integrity of the green part prior to debinding and sintering.

The strong effect of layer height suggests that the quality of the deposited structure plays a major role in the final behavior of the sintered specimens. Lower layer height resulted in the highest average tensile strength, which

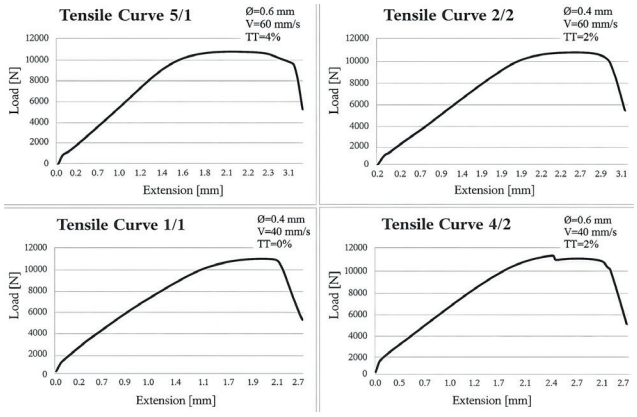


Fig. 11 Comparative tensile curves of higher- and lower-performing 17-4PH specimens illustrating the effect of internal heterogeneity on extension behavior

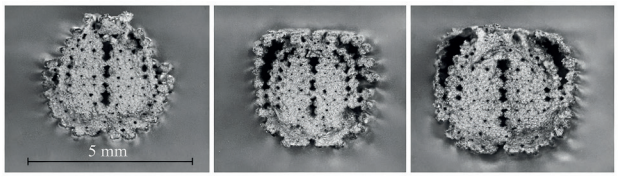


Fig. 12 Optical micrographs of fracture surfaces showing pores and incomplete bonding in 0.4 mm nozzle printed specimens

can be associated with a more favorable filament arrangement and more stable internal structure. Infill angle also had a clear influence, with 45° providing the best tensile response among the investigated conditions. This indicates that raster orientation affects not only the printed geometry, but also the way the structure consolidates and transfers load after sintering.

By contrast, printing speed showed a smaller effect within the examined range, suggesting that once a stable deposition window is achieved, the geometric arrangement of the deposited material becomes more important than deposition rate itself. The complementary dimensional and density-related results support this interpretation. The shrinkage measurements confirmed that dimensional contraction is substantial and should be treated as a process-dependent response.

The density-based evaluation further showed that sintering improved consolidation, but only to a limited extent. This means that post-processing can enhance the structure, but cannot fully compensate for insufficient packing quality or local discontinuities already present in the green part. This interpretation is reinforced by the fracture-surface observations. Visible pores, incomplete bonding, and local material-deficient regions indicate that internal heterogeneity remained a critical factor in the final specimens. The lower-performing samples also showed reduced elongation and less stable tensile behavior, which is consistent with the presence of structural defects acting as stress concentrators.

Taken together, these findings suggest that the measured tensile differences are best understood as the result of defect-sensitive process evolution rather than as the isolated effect of printing parameters alone. The best-performing specimen reached 802 MPa, corresponding to approximately 80% of the tensile strength reported by the material supplier. Considering that the specimens were tested in the as-sintered condition without machining or surface finishing, this result confirms the practical potential of the process. At the same time, the remaining difference from the supplier value is likely related to residual porosity, surface condition, and local discontinuities that were not fully eliminated during post-processing.

A limitation of the present study is the absence of direct volumetric defect characterization, such as X-ray CT or detailed metallographic sectioning. Therefore, the relative contributions of printing-induced heterogeneity and post-processing-induced defect evolution cannot be separated conclusively. Nevertheless, the combined tensile, shrinkage, density, and fracture-surface results provide a consistent basis for interpreting the process–property relationship in extrusion-based 17-4PH stainless steel.

6 Conclusion

This study investigated the effect of selected Fused Filament Fabrication parameters on the tensile behavior and dimensional change of 17-4PH stainless steel specimens produced from bound-metal filament and subsequently subjected to catalytic debinding and sintering. The results showed that the final mechanical response is not determined by the printing stage alone, but by the full process chain linking deposition, binder removal, densification, shrinkage, and defect evolution. The Taguchi-based evaluation identified layer height as the most influential parameter, followed by infill angle, while printing speed had the smallest effect within the investigated range.

The most favorable performance was obtained at low layer height and intermediate infill angle, and the best specimen reached a tensile strength of 802 MPa, corresponding to approximately 80% of the manufacturer-reported value, despite testing in the as-sintered and unmachined condition. The complementary dimensional, density-related, and fracture-surface results provided a more complete interpretation of these trends. Shrinkage measurements confirmed that dimensional contraction is substantial and process-dependent, while density analysis showed that sintering improves consolidation but does not fully compensate for insufficient green-part homogeneity. Fracture-surface observations revealed pores, incomplete bonding, and local structural discontinuities, indicating that internal heterogeneity is a major factor controlling tensile performance.

Taken together, the results demonstrate that the measured parameter effects should be interpreted through their influence on green-part integrity and subsequent post-processing sensitivity. Accordingly, the present work supports a process-chain-based understanding of extrusion-based metal additive manufacturing and contributes to the optimization of 17-4PH stainless steel processing by linking nominal printing parameters to the final defect-sensitive mechanical behavior of sintered parts.

References

Alami, A. H., Olabi, A. G., Alashkar, A., Alasad, S., Aljaghoub, H., Rezk, H., Abdelkareem, M. A. (2023) "Additive Manufacturing in the Aerospace and Automotive Industries: Recent Trends and Role in Achieving Sustainable Development Goals", Ain Shams Engineering Journal, 14(11), 102516. https://doi.org/10.1016/j.asej.2023.102516

Allahverdi, M., Danforth, S. C., Jafari, M., Safari, A. (2001) "Processing of Advanced Electroceramic Components by Fused Deposition Technique", Journal of the European Ceramic Society, 21, pp. 1485–1490. https://doi.org/10.1016/S0955-2219(01)00047-4

Cho, Y.-H., Park, S.-Y., Kim, J.-Y., Lee, K.-A. (2023) "17-4PH Stainless Steel with Excellent Strength–Elongation Combination Developed via Material Extrusion Additive Manufacturing", Journal of Materials Research and Technology, 24, pp. 3284–3299. https://doi.org/10.1016/j.jmrt.2023.03.228

Galantucci, L. M., Pellegrini, A., Guerra, M. G., Lavecchia, F. (2022) "3D Printing of Parts Using Metal Extrusion: An Overview of Shaping Debinding and Sintering Technology", Advanced Technologies & Materials, 47(1), pp. 25–32. https://doi.org/10.24867/ATM-2022-1-005

German, R. M. (2019) "Metal Powder Injection Molding (MIM): Key Trends and Markets", in Handbook of Metal Injection Molding. Elsevier, pp. 1–21. https://doi.org/10.1016/B978-0-08-102152-1.00001-5

Godec, D., Cano, S., Holzer, C., Gonzalez-Gutierrez, J. (2020) "Optimization of the 3D Printing Parameters for Tensile Properties of Specimens Produced by Fused Filament Fabrication of 17-4PH Stainless Steel", Materials, 13(3), 774. https://doi.org/10.3390/ma13030774

Henry, T. C., Morales, M. A., Cole, D. P., Shumeyko, C. M., Riddick, J. C. (2021) "Mechanical Behavior of 17-4 PH Stainless Steel Processed by Atomic Diffusion Additive Manufacturing", The International Journal of Advanced Manufacturing Technology, 114(7–8), pp. 2103–2114. https://doi.org/10.1007/s00170-021-06785-1

Kedziora, S., Decker, T., Museyibov, E., Morbach, J., Hohmann, S., Huwer, A., Wahl, M. (2022) "Strength Properties of 316L and 17-4 PH Stainless Steel Produced with Additive Manufacturing", Materials, 15(18), 6278. https://doi.org/10.3390/ma15186278

Ledniczky, Gy., Bognár, A., Kun, K., Zsidai, L., Weltsch, Z. (2024) "The Influence of the Process Parameters on the Mechanical Properties of Metal Specimens Produced by Fused Filament Fabrication", In: 39th Colloquium on Advanced Manufacturing and Repair Technologies in Vehicle Industry, Oficyna Wydawnicza Stowarzyszenia Menedzerow Jakosci i Produkcji, Czestochowa, Poland, ISBN 9788397041103

Liu, B., Wang, Y., Lin, Z., Zhang, T. (2020) "Creating Metal Parts by Fused Deposition Modeling and Sintering", Materials Letters, 263, 127252. https://doi.org/10.1016/j.matlet.2019.127252

Nurhudan, A. I., Supriadi, S., Whulanza, Y., Saragih, A. S. (2021) "Additive Manufacturing of Metallic Based on Extrusion Process: A Review", Journal of Manufacturing Processes, 66, pp. 228–237. https://doi.org/10.1016/j.jmapro.2021.04.018

Pellegrini, A., Lavecchia, F., Guerra, M. G., Galantucci, L. M. (2023) "Influence of Aging Treatments on 17–4 PH Stainless Steel Parts Realized Using Material Extrusion Additive Manufacturing Technologies", The International Journal of Advanced Manufacturing Technology, 126(1–2), pp. 163–178. https://doi.org/10.1007/s00170-023-11136-3

Singh, G., Missiaen, J.-M., Bouvard, D., Chaix, J.-M. (2021) "Additive Manufacturing of 17–4 PH Steel Using Metal Injection Molding Feedstock: Analysis of 3D Extrusion Printing, Debinding and Sintering", Additive Manufacturing, 47, 102287. https://doi.org/10.1016/j.addma.2021.102287

Suwanpreecha, C., Manonukul, A. (2022) "A Review on Material Extrusion Additive Manufacturing of Metal and How It Compares with Metal Injection Moulding", Metals, 12(3), 429. https://doi.org/10.3390/met12030429

Thompson, Y., Gonzalez-Gutierrez, J., Kukla, C., Felfer, P. (2019) "Fused Filament Fabrication, Debinding and Sintering as a Low-Cost Additive Manufacturing Method of 316L Stainless Steel", Additive Manufacturing, 30, 100861. https://doi.org/10.1016/j.addma.2019.100861

Wohlers Associates (2017) "Wohlers Report 2017: 3D Printing and Additive Manufacturing State of the Industry: Annual Worldwide Progress Report", Wohlers Associates, Washington, DC, USA. [online] https://wohlersassociates.com/product/wohlers-report-2017/

Wu, G., Langrana, N. A., Sadanji, R., Danforth, S. C. (2002) "Solid Freeform Fabrication of Metal Components Using Fused Deposition of Metals", Materials & Design, 23(1), pp. 97–105 https://doi.org/10.1016/S0261-3069(01)00079-6

Zhang, Y., Roch, A. (2022) "Fused Filament Fabrication and Sintering of 17-4PH Stainless Steel", Manufacturing Letters, 33, pp. 29–32. https://doi.org/10.1016/j.mfglet.2022.06.004

BASF ForwardAM (2023) Ultrafuse® 17-4PH Technical Data Sheet. Available at: https://forward-am.com